iScience

Article

High-throughput determination of protein affinities using unmodified peptide libraries in nanomolar scale

High-throughput peptide synthesis

Protein-derived peptide libraries

Overlapping libraries

Deep positional scans

Quasi label-free hit identification and affinity determination using TRIC

Fluorescence

Bound

Unbound

Time

Clemens Schulte,
Vladimir
Khayenko, Noah
Frieder
Nordblom,
Franziska Tippel,
Violetta Peck,
Amit Jean Gupta,
Hans Michael
Maric

hans.maric@uni-wuerzburg.de

HIGHLIGHTS
Protein affinity
determination via
temperature-related
intensity change (TRIC)

Tracer displacement
enables sensitive and
quasi-label-free
measurements in solution

Coupling to high-
throughput peptide
synthesis empowers
large-scaled screening

Largely automated hit
identification and affinity
determination in
nanomolar scale

iScience

Article

High-throughput determination of protein affinities using unmodified peptide libraries in nanomolar scale

Clemens Schulte,[1] Vladimir Khayenko,[1] Noah Frieder Nordblom,[1] Franziska Tippel,[2] Violetta Peck,[1] Amit Jean Gupta,[2] and Hans Michael Maric[1,3,*]

SUMMARY

Protein-protein interactions (PPIs) are of fundamental importance for our understanding of physiology and pathology. PPIs involving short, linear motifs play a major role in immunological recognition, signaling, and regulation and provide attractive starting points for pharmaceutical intervention. Yet, state-of-the-art protein-peptide affinity determination approaches exhibit limited throughput and sensitivity, often resulting from ligand immobilization, labeling, or synthesis. Here, we introduce a high-throughput method for in-solution analysis of protein-peptide interactions using a phenomenon called temperature related intensity change (TRIC). We use TRIC for the identification and fine-mapping of low- and high-affinity protein interaction sites and the definition of sequence binding requirements. Validation is achieved by microarray-based studies using wild-type and mutated recombinant protein and the native protein within tissue lysates. On-chip neutralization and strong correlation with structural data establish TRIC as a quasi-label-free method to determine binding affinities of unmodified peptide libraries with large dynamic range.

INTRODUCTION

Virtually all cellular processes involve protein-protein interactions (PPIs). A significant fraction of PPIs is dependent on short linear peptides, which are increasingly recognized for their roles in signaling and regulatory networks (Pawson and Nash, 2003) and antibody/antigen recognition (Brennan et al., 2010). Thus, they provide opportunities for therapeutic intervention and valuable starting points for the development of immunological biopharmaceuticals (Fosgerau and Hoffmann, 2015) and the design of PPI modulators (Christensen et al., 2020). Widely applied methods for the characterization and affinity determination of PPIs include peptide and protein microarrays (Lyamichev et al., 2017; Templin et al., 2002), surface plasmon resonance (SPR) (Patching, 2014), biolayer interferometry (BLI) (Sultana and Lee, 2015), isothermal calorimetry (ITC) (Ye and Wu, 2000), fluorescence polarization (FP) (Rooklin et al., 2017), and microscale thermophoresis (MST) (Duhr and Braun, 2006; Wienken et al., 2010). In tandem with high-throughput, nanomolar scale peptide synthesis (Frank, 1992; Sabatino and Papini, 2008), these technologies can be expected to simplify and accelerate protein-peptide interaction analysis and hence the development of pharmaceutical actuators.

Surface-based methods such as SPR, BLI, or array-based techniques provide high sensitivity and throughput. Yet, the required immobilization may affect molecular activity and limit affinity determination. On the other hand, label-free, in-solution affinity determination using ITC, although highly precise, does not allow for exhaustive screenings of large ligand libraries due to the limited sensitivity of calorimetric measurements and the resulting high sample consumption and limited throughput. Here, fluorescent readouts, such as MST and FP, are increasingly employed due to their largely reduced protein requirement, improving assay setup and high predictive value (Jerabek-Willemsen et al., 2011). When set up as displacement assays, they allow for quasi-label-free, in-solution affinity determination. The resulting possibility to use unmodified ligand libraries facilitates broader application. In such a setup, inhibitory constants (K_is) are determined by titration of unmodified competitive ligands to labeled protein-peptide complexes. Considerable automatization of sample preparation and their measurements and compatibility with small molecules, fragments, and peptides contributed to the increased application of FP for high-throughput

screening (Owicki, 2000). Yet, the FP phenomenon is dependent on ligand and size change upon binding as well as fluorophore and linker characteristics, thus requiring careful assay design (Zhang et al., 2015). In stark contrast, the MST phenomenon is largely independent of molecular weight changes, providing high dynamic range across different assay setups and probe designs (Gupta et al., 2018).

MST setups are highly sensitive; their automatization and miniaturization, however, have been limited by the requirement to track the molecular motion along a temperature gradient in a vessel that prevents turbulent flow (Linke et al., 2015). The dominating physical component of MST is the temperature-related intensity change (TRIC) of fluorescence, which is a measure for the decrease or increase of the fluorescence of a molecule in solution upon heating as a function of time. TRIC allows to detect interactions between target (typically a protein) and ligand with high sensitivity. The nature of the method requires ligand molecules to be non-fluorescent in the investigated red spectral range. Therefore, target molecules are commonly chemically modified with organic fluorophores (Gupta et al., 2018). Here, we explore the use of the Dianthus NT23.PicoDuo (Nanotemper Technologies GmbH) for TRIC measurements in reduced volumes of microtiter plates for affinity determination in unprecedented throughput while maintaining the advantages of conventional MST measurements.

RESULTS AND DISCUSSION

We conducted our measurements using the neuronal scaffold protein and master regulator of the inhibitory synapse gephyrin (Tyagarajan and Fritschy, 2014) (geph) and its structurally resolved interaction partners, the glycine receptor (GlyR) β subunit and the γ-aminobutyric acid type A receptor (GABA$_A$R) α3 subunit (Maric et al., 2011, 2014; Herweg and Schwarz, 2012). These receptor subunits bind to the E domain of geph (gephE) via a highly conserved linear binding motif. Geph mutations that affect these interactions disrupt the function of distinct synapse types (Hines et al., 2018; Nathanson et al., 2019) and result in neurological disorders (Dejanovic et al., 2014, 2015; Harvey et al., 2008). Low-affinity geph interactions (Brady and Jacob, 2015; Kowalczyk et al., 2013) could not be described for over three decades but were recently resolved thermodynamically (Herweg and Schwarz, 2012; Maric et al., 2011, 2014) and structurally (Kim et al., 2006; Maric et al., 2014) and were exploited to modulate neurotransmission (Maric et al., 2015, 2017; Hines et al., 2018; Kasaragod et al., 2019).

Peptide arrays enable high-throughput mapping of recombinant and native proteins

Peptide microarrays are among the most widely used formats to study antibody-epitope (Price et al., 2012) and peptide-mediated PPIs (Hilpert et al., 2005) in high-throughput. On-chip synthesis (Loeffler et al., 2016) and printable approaches such as Frank's SPOT method (Dikmans et al., 2006; Sereikaite et al., 2019; Hilpert et al., 2007) are among the most common and accessible techniques for microarray production. Here, we used μSPOT (Dikmans et al., 2006) to produce nanomolar scaled peptide stocks (Figure 1A) containing an overlapping GlyR β and GABA$_A$R α3 peptide library, which was subsequently printed in microarray format. Array titration with recombinant gephE (Figures 1B, 1C, and S1) recapitulates the structurally resolved (Maric et al., 2014) binding regions of the GlyR β and GABA$_A$R α3 subunit (^{420}FSIVG^{424} and ^{395}FNIVG^{399}, respectively). Importantly, the same setup also allows to study native geph within tissue lysates (Figures 1B and 1C). Titrations of the recombinant protein and the lysate yielded strongly correlating binding signals, thus indicating that endogenous levels of the protein are well within the dynamic range of this method and that protein expression and purification may not always be necessary for detailed protein binding studies. To circumvent antibody labeling of the native protein and enable the direct detection of the endogenous protein without further modification *in vitro*, we explored the use of lysates from knock-in mice expressing monomeric red fluorescent protein (mRFP)-geph in μSPOT format. The observed binding pattern showed high correlation to recombinant geph and the immunologically detected native geph but due to peptide autofluorescence and comparably poor quantum yield and photostability of the mRFP, this setup does not appear suitable for accurate affinity determination (Figure S2).

Validation of high- and low-affinity binding via on-chip neutralization

Major limitations of peptide-based techniques are false-positive and -negative signals resulting from immobilization, orientation, hydrophobicity, aggregation, and charge. Mapped binding sites were validated using known non-binding point-mutated gephE variants (Kim et al., 2006; Maric et al., 2011) (Figure S1B). Validation of specific binding is commonly achieved using binding impaired protein mutants. Yet, because peptide binding sites are often unknown and the prediction of mutations, genetic engineering, and protein repurification is laborious and often not feasible, we here explored alternative means of validation. Namely,
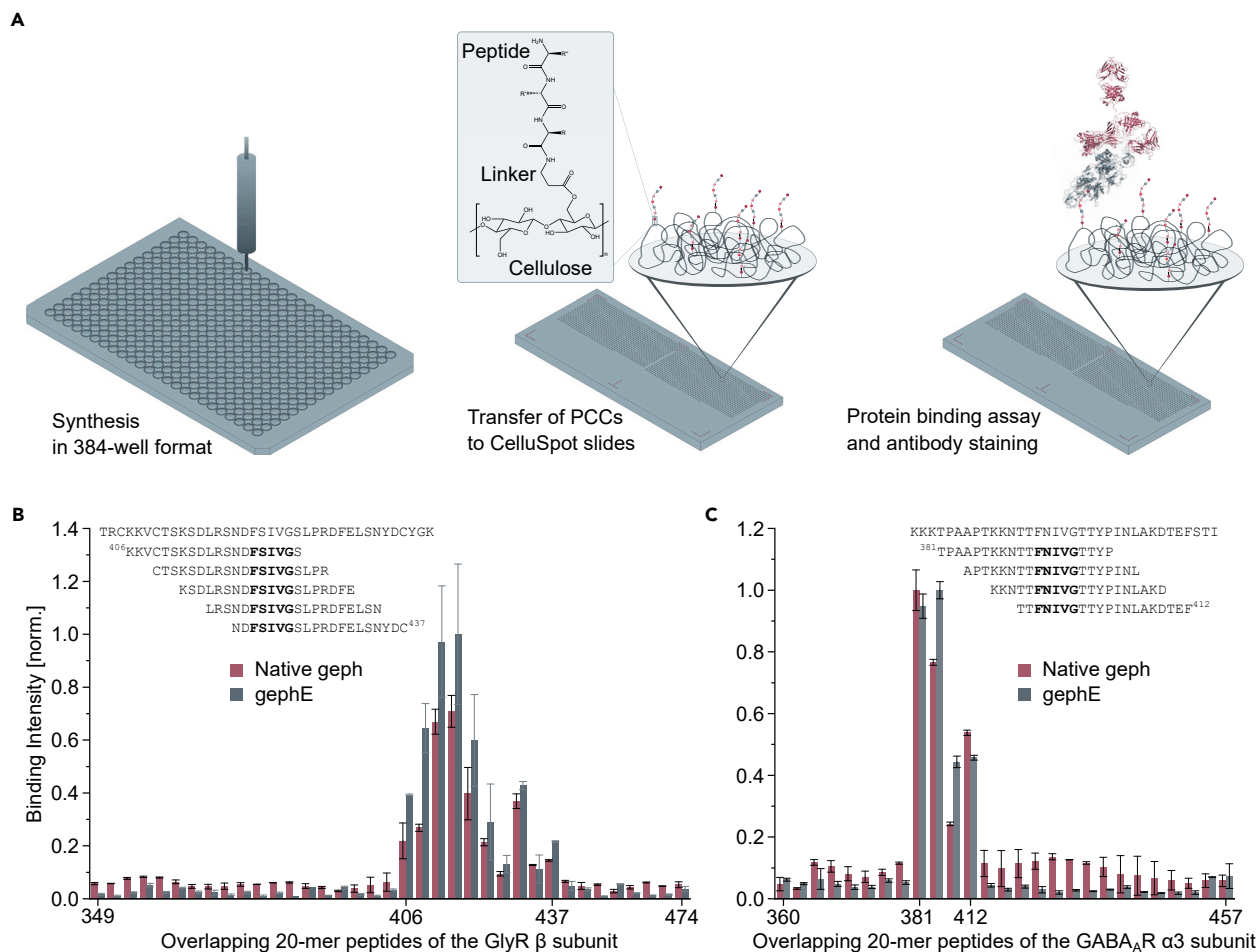
Figure 1. Microarray data

Mapping of native and recombinant protein binding sites.

(A) Microarray preparation. Up to 4 × 384 peptides are synthesized in parallel on cellulose using standard Fmoc solid-phase peptide synthesis. After sidechain deprotection and dissolution, peptide-cellulose conjugates are printed on coated slides and probed with proteins and their respective antibodies. The intracellular loops between TM 3 and 4 of the GlyR β (B) and the GABA$_A$R α3 subunit (C) were displayed via overlapping peptide libraries. Residues delimiting the peptides on-chip are represented on the x axis. Shown are relative binding intensities of native geph (3% and 6% lysate used for GlyR β and GABA$_A$R α3, respectively) and gephE (50 nM and 20 nM used for GlyR β and GABA$_A$R α3, respectively) for each individual peptide. Amino acid letter codes are displayed for prominent binders. Values are presented as n = 2 with array internal STDEV. Refer to Tables S1 and S2 for peptide sequences.

in situ on-chip peptide neutralization of binding signals (Figure S3). Adding µg amounts of peptides corresponding to the putative binding sites of the GlyRβ (FSIVGSLPRDFELC, **1a**) and the GABA$_A$R α3 subunit (FNIVGTTY, **1b**) effectively neutralizes the corresponding interaction (Figure S3). In addition, in line with the lower affinity of the GABA$_A$R α3- over the GlyR β-derived peptide, more peptide was needed to neutralize the high-affinity geph-GlyR β interaction (200 µM over 2 µM).

TRIC allows for sensitive affinity determination in-solution

To overcome the inherent caveats of array-based techniques, including immobilization-related artifacts resulting from peptide inactivation or unspecific accumulation of proteins depending on orientation, surface chemistry, and ligand density, we next explored the possibility to measure the same peptide library in-solution using TRIC. Compared with conventional MST setups, the here used TRIC setup allows for reduced sample volumes and is compatible with microtiter plates and thus facilitates higher throughput and automatization (Gupta et al., 2018). Large libraries of unmodified ligands are often analyzed with fluorescently labeled proteins. Here, Alexa 647-labeled gephE exhibited unspecific peptide binding (Figure S1A) as commonly observed. Among the tested alternative labeling strategies, Red-Maleimide second generation
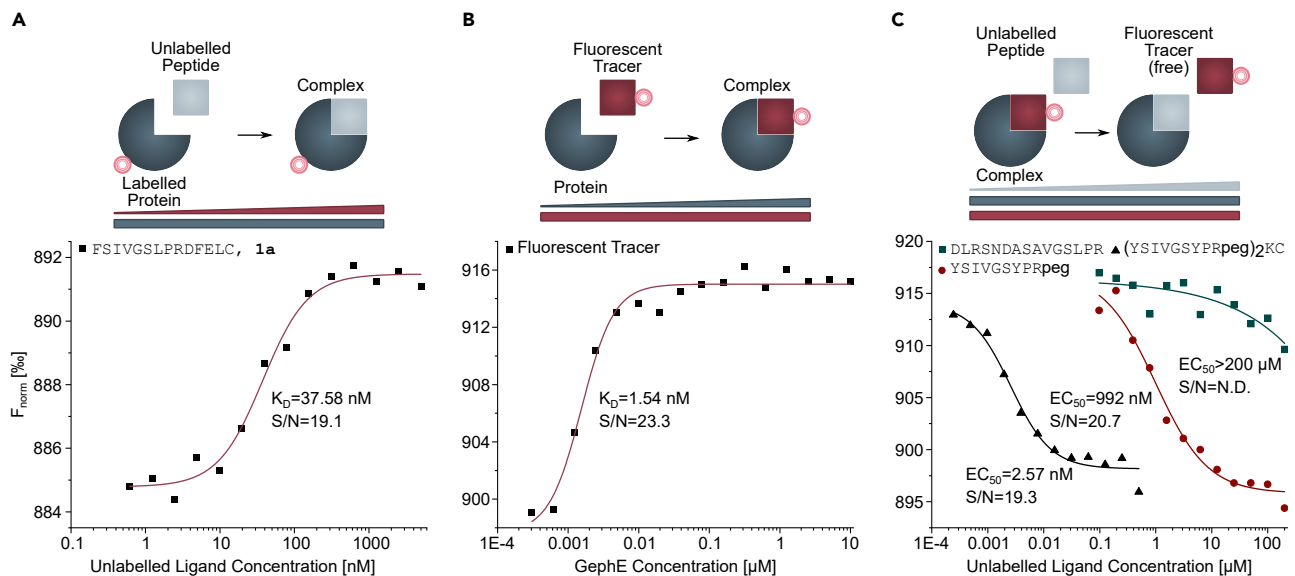
Figure 2. TRIC-based binding assays

(A) Red-Maleimide second generation-labeled gephE is titrated with increasing concentrations of an unlabeled, gephE-binding, GlyR β-derived peptide.

(B) A fluorescently labeled, dimeric geph-binding peptide is titrated with increasing concentrations of unlabeled gephE. Note that the F_{norm} signal amplitude is increased approximately two-fold in comparison to (A).

(C) A complex of unlabeled gephE with the fluorescent tracer is titrated with three unlabeled geph-binding peptides with varying affinity. TRIC measurements recapitulate the known hierarchy of monomeric and dimeric geph binding peptides.

(Nanotemper Technologies GmbH)-labeled gephE performed best (Figure 2A). Yet, the observed low-signal amplitude prompted us to explore alternative approaches for titrating unmodified peptides. To this end, we set up a displacement assay inspired by the on-chip neutralization strategy used for validating specific binding in microarray format (Figure S3). Specifically, we identified a high-affinity (K_D = 1.54 nM) fluorescently labeled tracer with enhanced TRIC response (Figure 2B). Displacement of this binder yields an inverse TRIC signal and enables the robust affinity determination of unmodified peptides (Figure 2C). Notably, the high-affinity dimeric fluorescent tracer (Maric et al., 2015) provides a large dynamic range for TRIC measurements, even when applied at nanomolar concentrations.

TRIC in tandem with high-throughput synthesis enables protein-peptide interaction screening

We envisioned that the accessible automated peptide synthesis setup that we used for screening in microarray format (Figure 1) could also empower the high-throughput screening of peptide libraries in solution using TRIC. First, a single-dose high-throughput screen was conducted. In this setup, each peptide is incubated with the gephE-tracer complex at a defined concentration in duplicate and subsequently measured. The temperature-dependent fluorescence in each well is monitored as a function of time, followed by the determination of the area between the resulting curves of each peptide and those of the control without competitor (Figure 3A and S5). Peptides exhibiting an area value above a defined threshold (here 0.5) are classified as binders. Peptides are assigned to the binders category after excluding false positives and false negatives. To this end, precipitation and air bubbles are detected by scans of each well in three axial directions. Furthermore, autofluorescence and fluorescence quenching artifacts are identified via additional steady-state fluorescence measurements. The recorded TRIC signal is additionally analyzed by an algorithm that classifies protein/peptide complexes as aggregated.

Here, an overlapping peptide library consisting of 15mer peptides with an offset of one amino acid was prepared to map the benchmark interaction of geph to the GlyR β (Figures 3B and S4A) and GABA_AR α3 (Figures 3C and S4B) subunit. The software (DI.ScreeningAnalysis Version 1.1.3, November 2020) conducted all described scans, calculations, and assignments automatically to successfully identify the structurally
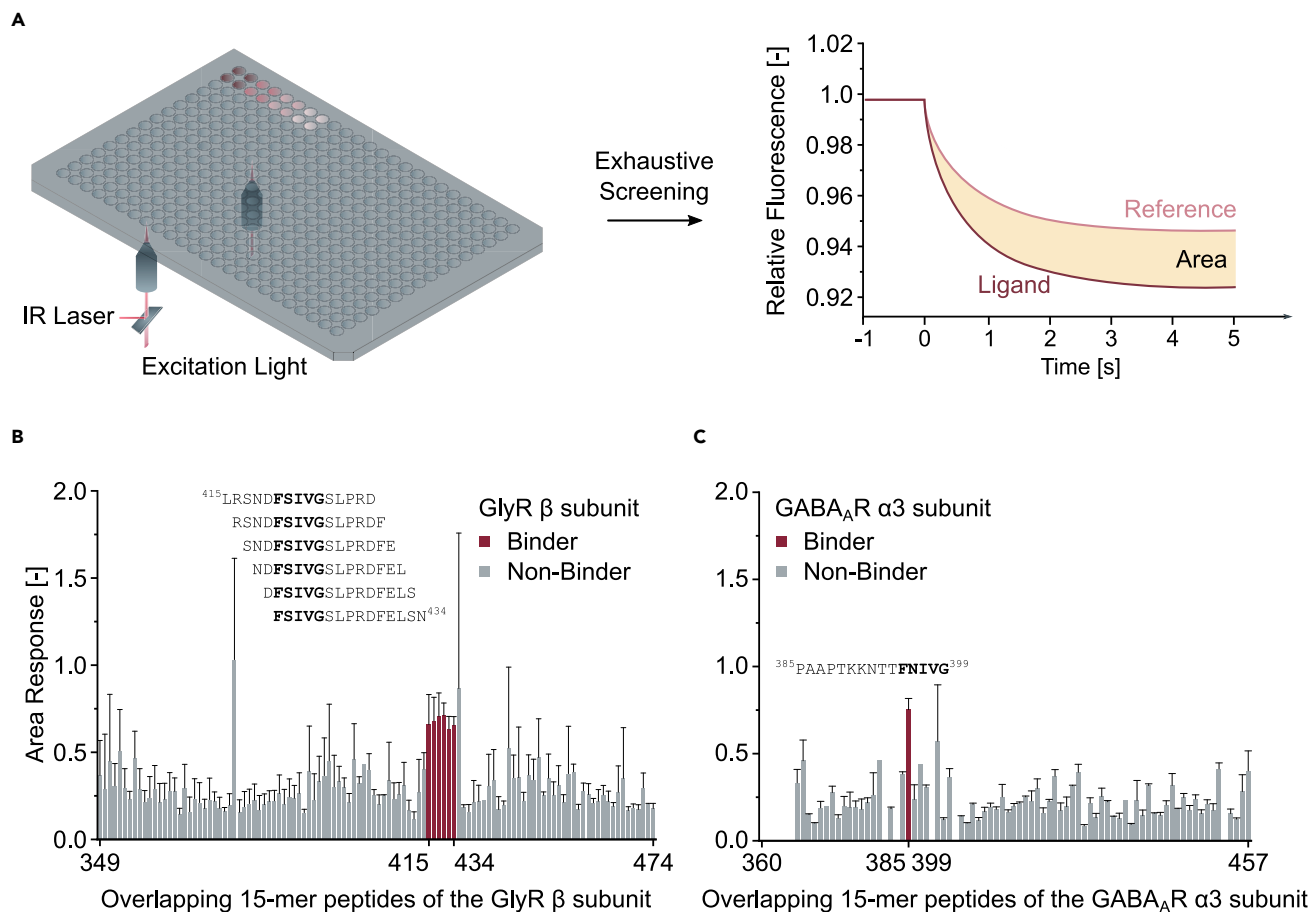
Figure 3. TRIC-based single-dose high-throughput screening

TRIC measurement applied for the exhaustive screening of peptide libraries in solution.

(A) Schematic representation of a single-dose TRIC setup. Two optical systems operate simultaneously below a 384-microtiter plate for increased throughput at a distance of nine wells. Unmodified peptides are typically screened as a duplicate. Binding is detected by calculating the area between signal traces recorded in presence and absence of the probed ligand.

(B and C) Bar graph showing area values for each peptide measured (see Tables S3 and S4 for peptide sequences corresponding to the GlyR β (B) and GABA$_A$R α3 (C) subunit respectively and area values for each data point). Residues delimiting the peptides on-chip are represented on the x axis. Hits are highlighted in dark red alongside corresponding peptide sequences with the respective binding motifs in bold. Note that the software gratifyingly classified sequences as binders that harbor the structurally resolved bindings sites [420]FSIVG[424] or [395]FNIVG[399] (GlyR β and GABA$_A$R α3 subunit respectively). Values are presented as n=1-6 with corresponding STDEV if applicable.

resolved (Maric et al., 2014) binding sites (Figures 3B and 3C), namely, [420]FSIVG[424] (GlyR β) and [395]FNIVG[399] (GABA$_A$R α3) bearing peptides.

High-throughput in-solution peptide-protein affinity determination using TRIC

Next, we aimed for the affinity determination of screened binders using the same setup and scale that we used for the single dose screen. To assess the reproducibility of the TRIC-based measurements, we subjected five independently synthesized GlyR β-derived peptides ([414]DLRSNDFSIVGSLPR[428]) to a twelve-point dose response measurement (Figure 4A). Here, two-fold increasing concentrations of the unlabeled peptide are incubated with a constant concentration of the gephE-tracer complex. The resulting K_i values (mean value: 12.1 ± 1.29 μM) showed low deviation between the median and mean value (Figures 4B and 4C). Thus, substantiating that precise affinity determination in this scale using the described setup is indeed feasible.

Comparison of microarray- and TRIC-based interaction profiles

Next, we combined TRIC measurements with high-throughput peptide synthesis to facilitate a more precise profiling of protein-peptide interactions. This was achieved by determination of residual affinities for
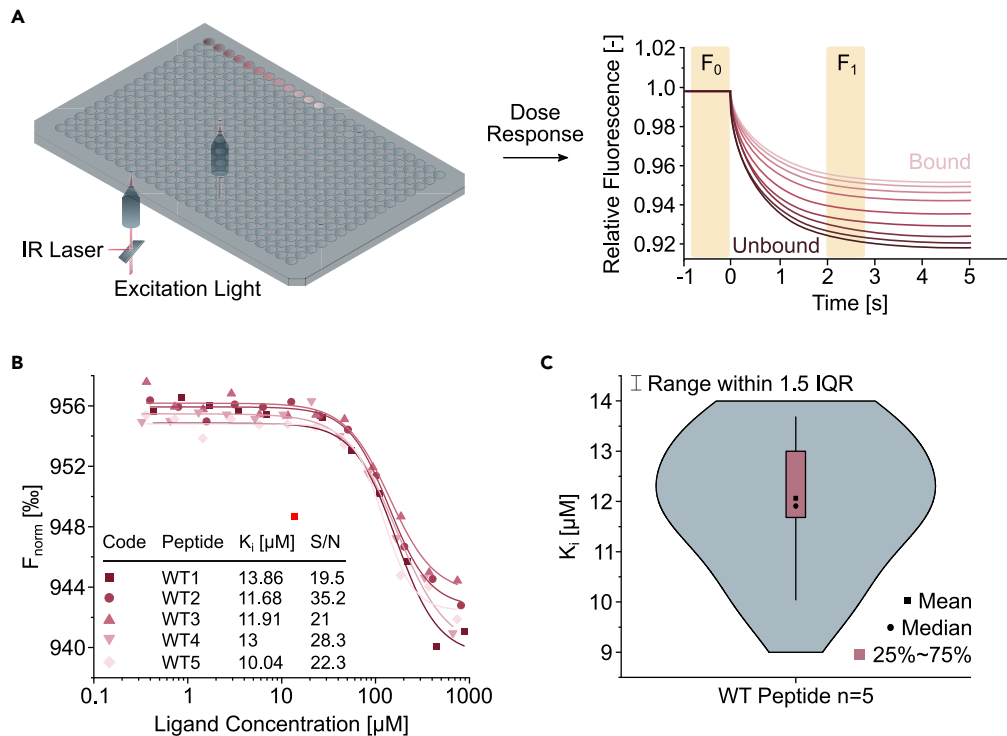
Figure 4. TRIC-based affinity determination

(A) Schematic representation of a dose response TRIC setup. Two optical systems operate simultaneously below a 384-microtiter plate for increased throughput at a distance of nine wells. Unmodified peptides are analyzed as a twelve-point dilution series with a dilution factor of two. The resulting TRIC traces are then analyzed for F_{norm} by comparison of the relative fluorescence at F_0 to F_1.

(B) Comparison of five independent measurements of a GlyR β-derived peptide (^{414}DLRSNDFSIVGSLPR^{428}) with respective K_i and S/N values. The bright red dot was identified as an outliner and excluded from curve fitting.

(C) Violin plot showing the mean EC_{50} value of the GlyR β-derived peptides in (B), alongside the mean, median, 25%–75% quantile and range within the 1.5 interquartile range (IQR). The high reproducibility indicates that TRIC-based affinity determination in nanomolar scale is feasible.

all possible point-mutated variants of the earlier resolved (Maric et al., 2014) benchmark geph—GlyR β and GABA$_A$R α3 interaction. First, the identified GlyR β binding motif was subjected to a full positional scan in μSPOT format. Here, each position of the binding sequence is systematically interchanged to define binding requirements and the contribution of each amino acid in the binding sequence. The copyability of μSPOT arrays facilitated the characterization of the isolated binding domain gephE (Figure 5A), full-length geph (FL-geph) (Figure 5B), and native geph from tissue lysate (Figures 5C and S2) by enabling the generation of 5,400 individual data points over 9 arrays. In each of these scans, the highly conserved and thus highly mutation sensitive GlyR β binding motif ^{420}FSIVG^{424} was robustly resolved. Thus, validating that protein profiling with molecular resolution can be achieved in this setup even without necessitating expression, purification, and dye-conjugation of the target protein (Figure 5C).

To demonstrate the throughput and accuracy of our new setup, we complemented the microarray data with the corresponding TRIC-based in-solution measurements. To this end, a full positional scan of the GlyR β-derived peptide ^{414}DLRSNDFSIVGSLPR^{428} with variations within the ^{420}FSIVG^{424} sequence was performed in TRIC-format. Binding affinities of peptide variants were determined by 12-step titrations (Figures 5D–5G, S6, and S7). Direct comparison of the in-solution determined K_i values with the relative binding intensities from the microarray (sequences highlighted in red in Figures 5A, 5D–5G, and S7) reveal a strong correlation. Importantly, the obtained affinities are in line with previously determined values and the structurally resolved interaction interface (Maric et al., 2011, 2014; Kim et al., 2006). These data suggest that the here described TRIC setup allows for the definition of protein binding profiles in high throughput at a level of detail that is usually only achieved by laborious and low-throughput PPI affinity determination approaches.
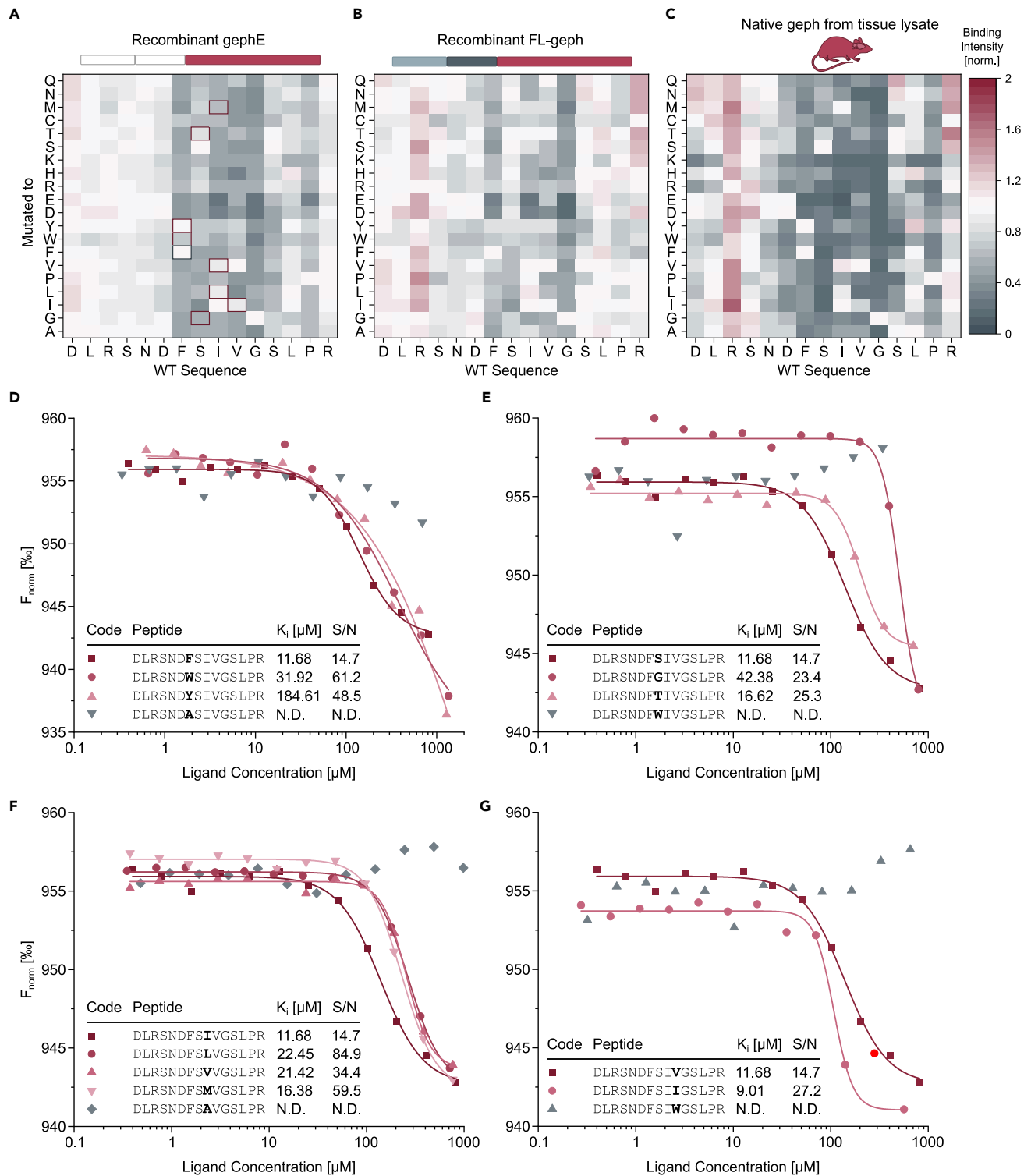
Figure 5. Comparison between binding profiles of GlyR β to gephE, FL-geph, and native Geph in μSPOT and TRIC format

(A) A full positional scanning library was probed with recombinant gephE, FL-geph (B), and native geph from tissue lysate (C) in microarray format. Geph domain architectures of the applied recombinant protein or lysate origin are indicated above the heatmaps. Shown are intensity values of point-mutated variants normalized to the corresponding WT sequence (GlyR β [414]DLRSNDFSIVGSLPR[428]) displayed as a heatmap. Higher spot intensity corresponds to

Figure 5. *Continued*

preferential binding, vice versa. In A, brackets corresponding to peptides that exhibited a determinable K_i value in TRIC format are bordered in red, whereas a representative WT sequence is bordered in blue. Values are presented as mean of n = 3. Refer to Table S5 for STDEV of each bracket. (D–G) Determined dose responses and derived K_i values of peptide variants in TRIC format. The interchanged position (position 420 (D), 421 (E), 422 (F) and 423 (G) of the GlyR β subunit respectively) is highlighted in bold. Peptides with a quantifiable K_i value are shown in red, alongside a representative non-binding variant in gray. Corresponding brackets in (A) are bordered in red. Bright red dots were excluded from curve fitting. Refer to Table S6 for starting concentrations of each peptide and Figure S7 for a direct comparison of the binding intensity found in microarray format and K_i values determined using TRIC.

DISCUSSION

This study defines TRIC as a novel and useful means for the high-throughput in-solution affinity determination of protein-ligand interactions. The setup was used for the rapid screening of 220 unmodified and nano-molar-scaled peptides and the immediate affinity determination of hits and all mutational variants that exhibit residual or enhanced binding. Using a displacement approach, we were able to boost the signal amplitude compared with measurements with a fluorescently labeled protein, while facilitating a quasi-label-free measurement of an unmodified peptide library. The obtained K_i values exhibited high reproducibility and correlated well with previously determined values (Maric et al., 2015). The binding data were complemented by conventional mapping and profiling using peptide microarrays, which are commonly employed for the characterization and mapping of protein-peptide interactions (Hilpert et al., 2005; Price et al., 2012). Here, we demonstrated that *ex vivo*-derived native protein within lysate can be used for direct microarray-based profiling studies. To overcome the required peptide immobilization that may introduce systematic biases, we employed TRIC to study the identical peptide libraries and demonstrate its use for screening as well as immediate affinity determination in solution. As such, this approach complements array-based approaches to provide molecular level characterization and furthermore provides a close-to-native measure of protein-peptide interaction strength that is usually only achieved after laborious and often low-throughput biophysical characterization.

In contrast to widely applied FP measurements, TRIC-based approaches provide higher flexibility regarding the properties and linkage of the fluorescent group. This is because only the fluorescent intensity upon temperature change is measured, whereas local mobility of the fluorophore does not influence the readout (Nasir and Jolley, 1999). The here described TRIC setup consumed around 50 ng protein, 2ng of the fluorescent tracer, and up to 700µg of studied peptide variant for a full 12-point dose response measurement. This enables its coupling to our high-throughput synthesis and thus any synthesis approach with the same nanomolar scaling including variants of Frank's highly accessible SPOT synthesis (Frank, 1992) as well as solid cellulose (Dikmans et al., 2006) or polystyrene bead-based (Murray et al., 2005) alternatives. Our approach allowed for synthesis of 768 or 384 peptides in parallel for single-dose measurements and 12-point dose responses, respectively. In addition to analysis of peptide binders that directly compete with the labeled tracer, the here presented setup also allows for the screening and subsequent affinity determination of small molecule and fragment libraries or even proteins and antibodies. Future studies may further emphasize on other applications that would be difficult to tackle with conventional binding assays including the ability of TRIC to detect binding events that do not cause a displacement of the fluorescently labeled tracer but rather result in the formation of a ternary complex. We expect that high-throughput TRIC measurements in combination with similar or alternative ligand library synthesis approaches will greatly accelerate the detailed mapping and characterization of binding sites and thereby help to decipher PPIs and their pharmaceutical targeting.

Limitations of the study

In the here presented work, we employ a displacement TRIC approach for the characterization of a benchmark PPI, which circumvents protein or ligand labeling and, at the same time, boosts the signal amplitude. Yet, the dynamic range of quantifiable affinities is limited by the affinity of the fluorescently labeled tracer peptide, similar to displacement setups using FP (Christensen et al., 2020). Consequently, to determine the affinity of lower affinity binders, the affinity of the tracer molecule would need to be adjusted accordingly. This will be crucial in fragment screenings, where the affinity determination of low-affinity fragments is of interest to maturate a high-affinity lead compound.

Peptide studies in solution are inherently limited by sequence-dependent aggregation, autofluorescence, and solubility. The here used TRIC setup allows to detect and subsequently exclude aggregation and autofluorescence and further ligand-induced fluorescence quenching by the peptide ligand (see Tables S3 and S4).

To fully exploit the throughput of TRIC measurements, we employed them in tandem with high-throughput μSPOT peptide synthesis followed by cleavage via a Rink-amide moiety. Although this approach is virtually unlimited with regard to possible peptide building blocks, this cleavage will leave peptides as terminal amides as do other commonly applied cleavage methods (Mcbride et al., 2016). Studies of PPIs that rely on interactions with C-terminal extremities, such as PDZ-domains (Christensen et al., 2019), may have to apply alternative cleavage strategies (Fraczyk et al., 2018). Here, we validated μSPOT synthesized peptides by LCMS and HPLC (Table S7) and determined the average purity of 15mers as 61 ± 24% and 47 ± 12% for 20mers. Accordingly, additional universal peptide purification steps could greatly enhance the robustness, sensitivity, and predictive value, especially for peptides exceeding 20 amino acids. Here, we employed preparatively synthesized and purified peptides for on-chip validation of signal specificity. To maintain high throughput, the on-chip neutralization could be adjusted so that peptides could be drawn from the same peptide stocks that are used for array printing.

Resource availability

Lead contact

Further information and requests for resources and reagents should be directed to and will be fulfilled by the Lead Contact, Hans Michael Maric (Hans.Maric@uni-wuerzburg.de).

Materials availability

There are restrictions to the availability of the fuorescent tracer due to the lack of an external centralized repository for its distribution and our need to maintain the stock. We are glad to share the fluorescent tracer with reasonable compensation by requestor for its processing and shipping.

Data and code availability

The published article includes all datasets generated or analyzed during this study.

METHODS

All methods can be found in the accompanying Tranparent methods.

SUPPLEMENTAL INFORMATION

Supplemental information can be found online at https://doi.org/10.1016/j.isci.2020.101898.

AUTHOR CONTRIBUTIONS

Conceptualization, H.M.M. and C.S.; Methodology, C.S., F.T., and A.J.G.; Investigation, C.S., F.T., and V.P.; Resources, V.K. and N.F.N.; Visualization, C.S.; Supervision, H.M.M., C.S., and V.K.; Writing—Original Draft, C.S. and H.M.M.; Writing—Review & Editing, C.S., H.M.M., A.J.G., and V.K.; Funding Acquisition, H.M.M; Administration, H.M.M.

DECLARATION OF INTERESTS

The authors declare no competing interests.

REFERENCES

Brady, M.L., and Jacob, T.C. (2015). Synaptic localization of α5 GABA (A) receptors via gephyrin interaction regulates dendritic outgrowth and spine maturation. Dev. Neurobiol. 75, 1241–1251.

Brennan, D.J., O'connor, D.P., Rexhepaj, E., Ponten, F., and Gallagher, W.M. (2010). Antibody-based proteomics: fast-tracking molecular diagnostics in oncology. Nat. Rev. Cancer 10, 605–617.

Christensen, N.R., Čalyševa, J., Fernandes, E.F.A., Lüchow, S., Clemmensen, L.S., Haugaard-Kedström, L.M., and Strømgaard, K. (2019). PDZ domains as drug targets. Adv. Ther. 2, 1800143.

Christensen, N.R., de Luca, M., Lever, M.B., Richner, M., Hansen, A.B., Noes-Holt, G., Jensen, K.L., Rathje, M., Jensen, D.B., and Erlendsson, S. (2020). A high-affinity, bivalent PDZ domain inhibitor complexes PICK 1 to alleviate neuropathic pain. EMBO Mol. Med. 12, e11248.

Dejanovic, B., Djemie, T., Grunewald, N., Suls, A., Kress, V., Hetsch, F., Craiu, D., Zemel, M., Gormley, P., Lal, D., et al. (2015). Simultaneous impairment of neuronal and metabolic function of mutated gephyrin in a patient with epileptic encephalopathy. EMBO Mol. Med. 7, 1580–1594.

Dejanovic, B., Lal, D., Catarino, C.B., Arjune, S., Belaidi, A.A., Trucks, H., Vollmar, C., Surges, R., Kunz, W.S., Motameny, S., et al. (2014). Exonic microdeletions of the gephyrin gene impair GABAergic synaptic inhibition in patients with idiopathic generalized epilepsy. Neurobiol. Dis. 67, 88–96.

Dikmans, A., Beutling, U., Schmeisser, E., Thiele, S., and Frank, R. (2006). SC2: a novel process for manufacturing multipurpose high-density chemical microarrays. Qsar Comb. Sci. 25, 1069–1080.

Duhr, S., and Braun, D. (2006). Why molecules move along a temperature gradient. Proc. Natl. Acad. Sci. 103, 19678–19682.

Fosgerau, K., and Hoffmann, T. (2015). Peptide therapeutics: current status and future directions. Drug Discov. Today 20, 122–128.

Fraczyk, J., Walczak, M., and Kaminski, Z.J. (2018). New methodology for automated SPOT synthesis of peptides on cellulose using 1, 3, 5-triazine derivatives as linkers and as coupling reagents. J. Pept. Sci. 24, e3063.

Frank, R. (1992). Spot-synthesis: an easy technique for the positionally addressable, parallel chemical synthesis on a membrane support. Tetrahedron 48, 9217–9232.

Gupta, A.J., Duhr, S., and Baaske, P. (2018). Microscale Thermophoresis (MST). In Encyclopedia of Biophysics, G. Roberts and A. Watts, eds. (Springer), pp. 1–5.

Harvey, R.J., Topf, M., Harvey, K., and Rees, M.I. (2008). The genetics of hyperekplexia: more than startle! Trends Genet. 24, 439–447.

Herweg, J., and Schwarz, G. (2012). Splice-specific glycine receptor binding, folding, and phosphorylation of the scaffolding protein gephyrin. J. Biol. Chem. 287, 12645–12656.

Hilpert, K., Volkmer-Engert, R., Walter, T., and Hancock, R.E. (2005). High-throughput generation of small antibacterial peptides with improved activity. Nat. Biotechnol. 23, 1008–1012.

Hilpert, K., Winkler, D.F., and Hancock, R.E. (2007). Peptide arrays on cellulose support: SPOT synthesis, a time and cost efficient method for synthesis of large numbers of peptides in a parallel and addressable fashion. Nat. Protoc. 2, 1333.

Hines, R.M., Maric, H.M., Hines, D.J., Modgil, A., Panzanelli, P., Nakamura, Y., Nathanson, A.J., Cross, A., Deeb, T., Brandon, N.J., et al. (2018). Developmental seizures and mortality result from reducing GABAA receptor alpha2-subunit interaction with collybistin. Nat. Commun. 9, 3130.

Jerabek-Willemsen, M., Wienken, C.J., Braun, D., Baaske, P., and Duhr, S. (2011). Molecular interaction studies using microscale thermophoresis. Assay Drug Dev. Technol. 9, 342–353.

Kasaragod, V.B., Hausrat, T.J., Schaefer, N., Kuhn, M., Christensen, N.R., Tessmer, I., Maric, H.M., Madsen, K.L., Sotriffer, C., Villmann, C., et al. (2019). Elucidating the molecular basis for inhibitory neurotransmission regulation by artemisinins. Neuron 101, 673–689 e11.

Kim, E.Y., Schrader, N., Smolinsky, B., Bedet, C., Vannier, C., Schwarz, G., and Schindelin, H. (2006). Deciphering the structural framework of glycine receptor anchoring by gephyrin. EMBO J. 25, 1385–1395.

Kowalczyk, S., Winkelmann, A., Smolinsky, B., Förstera, B., Neundorf, I., Schwarz, G., and Meier, J.C. (2013). Direct binding of GABAA receptor β2 and β3 subunits to gephyrin. Eur. J. Neurosci. 37, 544–554.

Linke, P., Amaning, K., Maschberger, M., Vallee, F., Steier, V., Baaske, P., Duhr, S., Breitsprecher, D., and Rak, A. (2015). An automated microscale thermophoresis screening approach for fragment-based lead discovery. J. Biomol. Screen. 21, 414–421.

Loeffler, F.F., Foertsch, T.C., Popov, R., Mattes, D.S., Schlageter, M., Sedlmayr, M., Ridder, B., Dang, F.-X., von Bojničić-Kninski, C., Weber, L.K., et al. (2016). High-flexibility combinatorial peptide synthesis with laser-based transfer of monomers in solid matrix material. Nat. Commun. 7, 11844.

Lyamichev, V.I., Goodrich, L.E., Sullivan, E.H., Bannen, R.M., Benz, J., Albert, T.J., and Patel, J.J. (2017). Stepwise evolution improves identification of diverse peptides binding to a protein target. Sci. Rep. 7, 12116.

Maric, H.-M., Mukherjee, J., Tretter, V., Moss, S.J., and Schindelin, H. (2011). Gephyrin-mediated γ-aminobutyric acid type A and glycine receptor clustering relies on a common binding site. J. Biol. Chem. 286, 42105–42114.

Maric, H.M., Hausrat, T.J., Neubert, F., Dalby, N.O., Doose, S., Sauer, M., Kneussel, M., and Stromgaard, K. (2017). Gephyrin-binding peptides visualize postsynaptic sites and

modulate neurotransmission. Nat. Chem. Biol. 13, 153–160.

Maric, H.M., Kasaragod, V.B., Haugaard-Kedström, L., Hausrat, T.J., Kneussel, M., Schindelin, H., and Strømgaard, K. (2015). Design and synthesis of high-affinity dimeric inhibitors targeting the interactions between gephyrin and inhibitory neurotransmitter receptors. Angew. Chem. Int. Ed. 54, 490–494.

Maric, H.M., Kasaragod, V.B., Hausrat, T.J., Kneussel, M., Tretter, V., Strømgaard, K., and Schindelin, H. (2014). Molecular basis of the alternative recruitment of GABA A versus glycine receptors through gephyrin. Nat. Commun. 5, 1–11.

Mcbride, R., Head, S.R., Ordoukhanian, P., and Law, M. (2016). Low-cost Peptide Microarrays for Mapping Continuous Antibody Epitopes. Peptide Microarrays (Springer).

Murray, J.K., Farooqi, B., Sadowsky, J.D., Scalf, M., Freund, W.A., Smith, L.M., Chen, J., and Gellman, S.H. (2005). Efficient synthesis of a β-peptide combinatorial library with microwave irradiation. J. Am. Chem. Soc. 127, 13271–13280.

Nasir, M.S., and Jolley, M.E. (1999). Fluorescence polarization: an analytical tool for immunoassay and drug discovery. Comb. Chem. High Throughput Screen. 2, 177–190.

Nathanson, A.J., Zhang, Y., Smalley, J.L., Ollerhead, T.A., Santos, M.A.R., Andrews, P.M., Wobst, H.J., Moore, Y.E., Brandon, N.J., and Hines, R.M. (2019). Identification of a core amino acid motif within the α subunit of GABAARs that promotes inhibitory synaptogenesis and resilience to seizures. Cell Rep. 28, 670–681. e8.

Owicki, J.C. (2000). Fluorescence polarization and anisotropy in high throughput screening: perspectives and primer. J. Biomol. Screen. 5, 297–306.

Patching, S.G. (2014). Surface plasmon resonance spectroscopy for characterisation of membrane protein–ligand interactions and its potential for drug discovery. Biochim. Biophys. Acta 1838, 43–55.

Pawson, T., and Nash, P. (2003). Assembly of cell regulatory systems through protein interaction domains. science 300, 445–452.

Price, J.V., Tangsombatvisit, S., Xu, G., Yu, J., Levy, D., Baechler, E.C., Gozani, O., Varma, M., Utz, P.J., and Liu, C.L. (2012). On silico peptide microarrays for high-resolution mapping of antibody epitopes and diverse protein-protein interactions. Nat. Med. 18, 1434.

Rooklin, D., Modell, A.E., Li, H., Berdan, V., Arora, P.S., and Zhang, Y. (2017). Targeting unoccupied surfaces on protein–protein interfaces. J. Am. Chem. Soc. 139, 15560–15563.

Sabatino, G., and Papini, A.M. (2008). Advances in automatic, manual and microwave-assisted solid-phase peptide synthesis. Curr. Opin. Drug Discov. Dev. 11, 762.

Sereikaite, V., Fritzius, T., Kasaragod, V.B., Bader, N., Maric, H.M., Schindelin, H., Bettler, B., and Strømgaard, K. (2019). Targeting the γ-aminobutyric acid type B (GABAB) receptor complex: development of inhibitors targeting the K+ channel tetramerization domain (KCTD) containing proteins/GABAB receptor protein–protein interaction. J. Med. Chem. 62, 8819–8830.

Sultana, A., and Lee, J.E. (2015). Measuring protein-protein and protein-nucleic acid interactions by biolayer interferometry. Curr. Protoc. Protein Sci. 79, 19.25.1–19.25.26.

Templin, M.F., Stoll, D., Schrenk, M., Traub, P.C., Vöhringer, C.F., and JOOS, T.O. (2002). Protein microarray technology. Drug Discov. Today 7, 815–822.

Tyagarajan, S.K., and Fritschy, J.M. (2014). Gephyrin: a master regulator of neuronal function? Nat. Rev. Neurosci. 15, 141–156.

Wienken, C.J., Baaske, P., Rothbauer, U., Braun, D., and Duhr, S. (2010). Protein-binding assays in biological liquids using microscale thermophoresis. Nat. Commun. 1, 100.

Ye, H., and Wu, H. (2000). Thermodynamic characterization of the interaction between TRAF2 and tumor necrosis factor receptor peptides by isothermal titration calorimetry. Proc. Natl. Acad. Sci. U S A 97, 8961–8966.

Zhang, H., Wu, Q., and Berezin, M.Y. (2015). Fluorescence anisotropy (polarization): from drug screening to precision medicine. Expert Opin. Drug Discov. 10, 1145–1161.

Supplemental Information

High-throughput determination of protein

affinities using unmodified peptide

libraries in nanomolar scale

Clemens Schulte, Vladimir Khayenko, Noah Frieder Nordblom, Franziska Tippel, Violetta Peck, Amit Jean Gupta, and Hans Michael Maric

Supplemental Information

High-throughput Determination of Protein Affinities using Unmodified Peptide Libraries in Nanomolar Scale

Clemens Schulte[1]; Vladimir Khayenko[1]; Noah Frieder Nordblom[1]; Franziska Tippel[2], Violetta Peck[1]; Amit Jean Gupta[2]; Hans Michael Maric[1]*

[1]Rudolf Virchow Center; Center for Integrative and Translational Bioimaging; University of Wuerzburg; Josef-Schneider-Str. 2, Germany, 97080 Wuerzburg, Germany

[2]Nanotemper Technologies GmbH, Flößergasse 4, 81369 Munich, Germany

Transparent Methods

Unless otherwise stated, amino acids and reagents were purchased from either Iris Biotech or Carl Roth. All solvents were purchased from commercial sources and used without further purification.

Automated Solid-Phase Peptide Synthesis

µSPOT peptide arrays(Dikmans et al., 2006) (CelluSpots, Intavis AG, Cologne, Germany) were synthesized using a MultiPep RSi robot (Intavis AG) on in-house produced, acid labile, amino functionalized, cellulose membrane discs containing 9-fluorenylmethyloxycarbonyl-β-alanine (Fmoc-β-Ala) linkers (average loading: 131 nmol/disc – 4 mm diameter). Synthesis was initiated by Fmoc deprotection using 20% piperidine (pip) in dimethylformamide (DMF) followed by washing with DMF and ethanol (EtOH). Peptide chain elongation was achieved using a coupling solution consisting of preactivated amino acids (aas, 0.5 M) with ethyl 2-cyano-2-(hydroxyimino)acetate (oxyma, 1 M) and N,N'-diisopropylcarbodiimide (DIC, 1 M) in DMF (1:1:1, aa:oxyma:DIC). Couplings were carried out for 3×30 min, followed by capping (4% acetic anhydride in DMF) and washes with DMF and EtOH. Synthesis was finalized by deprotection with 20% pip in DMF (2×4 µL/disc for 10 min each), followed by washing with DMF and EtOH. Dried discs were transferred to 96 deep-well blocks and treated, while shaking, with sidechain deprotection solution, consisting of 90% trifluoracetic acid (TFA), 2% dichloromethane (DCM), 5% H_2O and 3% triisopropylsilane (TIPS) (150 µL/well) for 1.5 h at room temperature (rt). Afterwards, the deprotection solution was removed, and the discs were solubilized overnight (ON) at rt, while shaking, using a solvation mixture containing 88.5% TFA, 4% trifluoromethanesulfonic acid (TFMSA), 5% H_2O and 2.5% TIPS (250 µL/well). The resulting peptide-cellulose conjugates (PCCs) were precipitated with ice-cold ether (0.7 mL/well) and spun down at 2000×g for 10 min at 4 °C, followed by two additional washes of the formed pellet with ice-cold ether. The resulting pellets were dissolved in DMSO (250 µL/well) to give final stocks. PCC solutions were mixed 2:1 with saline-sodium citrate (SSC) buffer (150 mM NaCl, 15 mM trisodium citrate, pH 7.0) and transferred to a 384-well plate. For transfer of the PCC solutions to white coated CelluSpot blank slides (76×26 mm, Intavis AG), a SlideSpotter (Intavis AG) was used. After completion of the printing procedure, slides were left to dry ON.

Peptides used for MST measurements were synthesized using a cleavable amide linker. After synthesis, cellulose disks were transferred to 96 deep-well blocks and treated with

sidechain deprotection solution for 3 hrs at rt under agitation. The solution was subsequently transferred to new 96 deep-well plates and 700 µL ice cold ether were added to each well. After ON precipitation of the peptides at -20 °C, the 96 deep-well blocks were centrifuged at 2,000 xG for 30 min and the supernatant (SN) was discarded. After an additional wash with 700 µL ice cold ether, peptides were solubilized in MST assay buffer consisting of 1×phosphate-buffered saline (PBS; 137 mM NaCl, 2.7 mM KCl, 10 mM Na_2HPO_4, 1.8 mM KH_2PO_4, pH 7.4) with 0.1% Pluronic F-127 (5% solution, Nanotemper Technologies GmbH) and 2 mM reduced L-Glutathione (GSH, Sigma-Aldrich G4251).

Preparative Peptide Synthesis

Standard solid phase peptide synthesis with Fmoc chemistry was applied, shortly, 2-chlorotrityl resin (1.6 mmol/g) was swollen in dry DCM for 30 min., then, the desired aa (1eq) and the orthogonally protected Boc-Gly-OH (1eq) with 2 eq. of dry N,N-Diisopropylethylamine (DIEA) were added to the resin slurry. Boc-Gly-OH was added to reduce resin loading to prevent aggregation of the growing peptide chain. After ON reaction, the resin was capped with MeOH and washed with DCM and DMF. Deprotection and conjugation cycles followed, where 20% pip solution in DMF was used to remove the Fmoc protecting group, and after washes the peptide chain was elongated by adding aa (3eq.) with oxyma (3eq.) and DIC (3eq.). Coupling efficiency was monitored by measuring the absorption of the dibenzofulvene–pip adduct after deprotection. The peptides were cleaved from the resin using a cocktail of 82.5% TFA, 5% phenol, 5% H_2O, 5% thioanisole, 2.5% 1,2-ethanedithiol for 4 h at rt. The peptides were precipitated in ice-cold ether and then purified with high performance liquid chromatography (HPLC) and analysed by liquid chromatography-mass spectrometry (LCMS).

Protein Labeling

The protein construct of gephE (residues 318-736) was generated as previously described(Maric et al., 2014). Labeling with Alexa Fluor™ 647 NHS-Ester (Succinimidylesther) was achieved using a labelling kit (Invitrogen, A37573) according to the manufacturer's instructions. Labeling with Red-Maleimide 2nd generation was achieved using a labelling kit (Nanotemper, MO-L014) according to the manufacturer's instructions.

Preparation of Mouse Tissue Lysates

Whole mouse brains were obtained from C57BL/6J mice at >4 weeks of age and immediately flash frozen in liquid N_2. Tissue of mRFP-gephyrin knock-in animals of 1 year of age (provided by Christian Specht, IBENS, Paris) was processed the same way. Before lysis, whole mouse brains were weighted and cut into four pieces along the coronal and sagittal axis. For preparation of one lysate, two diagonally opposite pieces were transferred into a 1.5 mL reaction tube (Sarsted). Lysis was carried out on ice in 400 µL RIPA lysis buffer (150 mM NaCl, 50 mM Tris-HCl (pH=8), 1% Nonident P-40 substitute, 0.5% DOC, 0.1% SDS (all v/v)), to which Ethylenediaminetetraacetic acid (5 mM end concentration) and 1 mini tablet of ROCHE complete protease inhibitor per 10 mL was added immediately before use, by hand crushing the brain material with a hand pestle in a 1.5 mL reaction tube. Lysis was completed by 1 min sonification on ice with a Sartorius Labsonic M Sonificator at 20% amplitude with care to avoid heating the suspensions. Finally, Lysates were centrifuged for 15 min at 17,200×g and 4 °C. The SN was subsequently collected, transferred to a new 1.5 mL reaction tube, flash frozen in liquid N_2 and stored at -80 °C until use.

Microarray Binding Assay

95 µSPOT slides were blocked by incubation with 2.5 mL 2% (w/v) IGG free bovine serum albumin (BSA) in PBS for 60 min at ~50 rpm and RT. Afterwards, slides were incubated with gephE or FL-geph at the desired concentration in 0.1% BSA in 1 × PBS for 30 min before slides were washed with 6×2.5 mL 1×PBS for 5 min. To label proteins for detection, the slides were incubated with 2.5 mL of a 1:10,000 diluted primary antibody (anti-gephyrin

100 (3B11, SynapticSystems) in 0.1% BSA in 1×PBS for 30 min, after which the slides were washed with 6×2.5 mL 1×PBS for 5 min. Afterwards, the slides were incubated with a secondary HRP-coupled Anti-mouse antibody (31430, Invitrogen) in 0.1% BSA in 1×PBS for 30 min, after which the slides were washed with 6×2.5 mL 1×PBS for 5 min. Peptide binding was detected through chemiluminescent detection (Lowest Sensitivity, 10s exposure time)

105 after application of 200 µL of SuperSignal West Femto Maximum Sensitive Substrate (Thermo Scientific) per slide using a c400 imaging system (Azure). Fluorescent detection (Cy3 channel, 700 V PMT, 25 µm pixel size, L5 latitude) as shown in Supplementary Figure 2 A was done using a Typhoon FLA 7000 scanner-based detection system (GE Healthcare).

Binding assays using fluorescently labelled gephyrin were performed similarly, without
110 antibody staining. Peptide binding was detected through fluorescence detection (60 µm resolution, 10s exposure time) on a c400 imaging system (Azure).

For on-chip peptide competition assays, gephE was preincubated with either peptide **1a** or **1b** in 0.1% BSA in PBS for 30 min on ice before being put on an array slide.

Binding intensities were evaluated using FIJI including the Microarray Profile addon
115 (OptiNav). After background subtraction of the mean greyscale value of the microarray surface surrounding the spots, raw greyscale intensities for each position were obtained for the left and right side of the internal duplicate on each microarray slide. The standard deviation (STDEV) between both sides was obtained using formula (1).

$$STDEV = \sqrt{\frac{\sum(x - \bar{x})}{n}} \tag{1}$$

with

n The total number of data points
$\bar{x}$ The mean intensity value

120

Afterwards, the raw spot intensities and corresponding STDEVs were normalized to the most prominent spot within the region of interest on the array. Data normalization for representation of a heatmap as in Figure 5 A, B, C was performed lane-wise, while normalization as in Supplementary Figure 2 B was performed to the average of all 15
125 wildtype-sequence peptides due to the comparably low spot intensity (Supplementary Figure 2 A).

Temperature Related Intensity Change (TRIC) Assays

An assay buffer consisting of 1× PBS (pH 7.4), 2 mM L-Glutathione reduced (GSH) and 0.1
130 % Pluronic F127 was used for all experiments. Before the measurements, all peptides were solubilized in assay buffer to an end concentration of 500-700 µM. The unlabelled control peptide NND1 was dissolved in the same buffer to a concentration of 4 µM. A HAMILTON STARlet system was used for liquid handling.

For single dose measurements, peptides were first diluted from the stock solution into assay
135 buffer to a 1:1 dilution in a conventional 384-microwell plate. In a second step, peptides were

mixed with the preincubated (1h at 4°C) target complex-containing solution consisting of gephE and NN1D-Alexa647, resulting in a final concentration of 20 nM and 10 nM respectively. This step took place in a Dianthus 384-microwell plate, in which the measurements were performed.

140 For 12-point affinity measurements, peptide solutions were first pre-diluted 1:1 in assay buffer, from which 0.5-fold dilutions were prepared in assay buffer in a standard 384-well plate. 15 µl of these dilutions were then mixed with 5 µl of target complex-containing assay buffer in a Dianthus 384-well plate, resulting in a final concentration of 5 nM gephE-NN1D-Alexa647 complex.

145 After the Dianthus 384-well microplates were loaded with the peptide and gephyrin-NN1D-Alexa647 complex, they were equilibrated for 16h at 4 °C and subsequently centrifuged for 30 sec at 1000×g immediately before starting the measurement in the Dianthus NT.23PicoDuo. The system was set to 25°C as set temperature. The samples were first measured for 1 sec without heating and for 5 sec with the IR-laser turned on. The two optical
150 systems in Dianthus were used in parallel, resulting in an overall measurement time of ~30 min per plate. Measured fluorescence values collected are displayed as relative fluorescence, where the fluorescence obtained at ambient temperature is normalized to one, and as normalized fluorescence (F_{norm}) which describes the ratio between fluorescence values (F1) after and the fluorescence values (F0) prior to IR laser activation and is typically
155 given in ‰. K_i values were obtained by applying a Hill-fit to a plot of F_{norm} vs. ligand concentration to determine an EC_{50} value, which was subsequently used to calculate the corresponding K_i value (Formula 2 and 3).

$$K_i = \frac{K_d}{2 - \gamma} \cdot \left(\frac{EC_{50}}{\frac{[T]_t}{\gamma} - \frac{K_d}{2 - \gamma} - \frac{[C]_t}{2}} - \gamma \right) \tag{2}$$

with

$$\gamma = \frac{[T]_t + [C]_t + K_d - \sqrt{([T]_t + [C]_t + K_d)^2 - 4[T]_t[C]_t}}{2[C]_t} \tag{3}$$

and

$[T]_t$ The total final concentration of the unlabelled target (gephE) in the assay
$[C]_t$ The total final concentration of fluorescent tracer (NN1D) in the assay that forms a complex with the target and is replaced by an unlabelled peptide ligand
K_d The K_d between the fluorescent tracer and the target from a direct binding affinity measurement
EC_{50} The EC_{50} obtained from titrating an unlabelled peptide ligand against the preformed complex of target and tracer

160

To provide a measure for the robustness of the dose response fits, the signal to noise ratio (S/N) was calculated from the signal amplitude of each fit and the residual values of all datapoints (Formula 4).

$$S/N = \frac{Signal\ Amplitude}{STDEV(Residuals)} \tag{4}$$

165 In the case of single dose measurements, the area response including all measured datapoints of the TRIC traces was considered instead of the F_{norm} value at a given timepoint. Here, the average area between the TRIC curve of the peptide ligand and the respective reference (no competitor peptide) is considered. Analysis of single-dose assays starts with the assignment of reference groups. A reference group designates a group of wells that are

4

all referenced together. In other words, the ligands within one reference group are compared to the same designated set of reference wells (wells with target protein but without ligand added). Next, the area between the traces obtained from all wells containing a reference sample are compared to one another. That results in a number of $((n^2-n)/2)$ areas, where n denotes the number of references. From these area values the mean reference area for that reference group is calculated. This procedure is repeated for all reference groups to yield their respective reference areas. The hit threshold is calculated in the following way (Formula 5):

$$Hit\ Threshold = m + z \cdot MAD \tag{5}$$

with

   m Median of all reference group areas in the assay
   z User-defined Z-score factor (7 in this study)
  MAD Median absolute deviation of all reference group areas in the assay

Next, for each ligand well (that contains ligand and labeled target) the area between the TRIC trace of that well to all reference wells in the same reference group is calculated and averaged to yield a mean signal area value for that well. If multiple wells were measured per ligand (in this screen a duplicate was measured) the area values per well are averaged to yield an average area per ligand. If this ligand-specific signal area exceeds the hit threshold, the ligand is considered a hit, provided that the software did not identify other issues like ligand-induced fluorescence quenching or aggregation. Furthermore, the area between individual repeats for each ligand, the ligand area, is calculated. This area will indicate whether a given ligand yields a reproducible signal. From all relevant areas for one ligand, reference area, signal area and ligand area the software calculates a signal quality value that is generally a very robust measure for the signal-to-noise that is obtained for a given ligand. This signal quality is calculated in the following way (Formula 6).

$$Signal\ Quality = \frac{\overline{Area_{Signal}}}{\dfrac{(\overline{Area_{Reference}} + \overline{Area_{Ligand}})}{2}} \tag{6}$$

Supplemental Figures
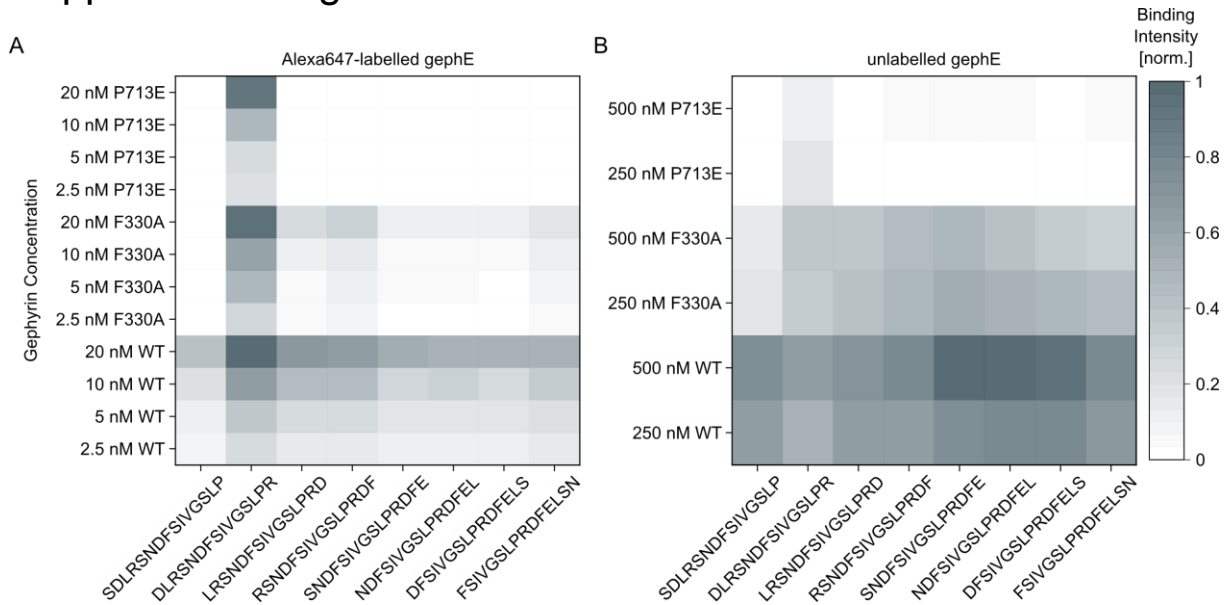
Supplemental Figure 1: Fluorescently labelled geph displays unspecific binding. Related to Figure 1. (A) Normalized binding intensities of Alexa647-labelled geph to GlyR β-derived peptides in µSPOT format. Note that for a certain peptide sequence ([414]DLRSNDFSIVGSLPR[428]), the binding intensity of fluorescently labelled WT geph is comparable to the binding intensity of two non-binding variants of gephE (F330A and P713E). (B) unlabelled gephE does not exhibit unspecific binding. Here, the relative binding intensity of WT geph is the highest overall, followed by F330A and P713E.
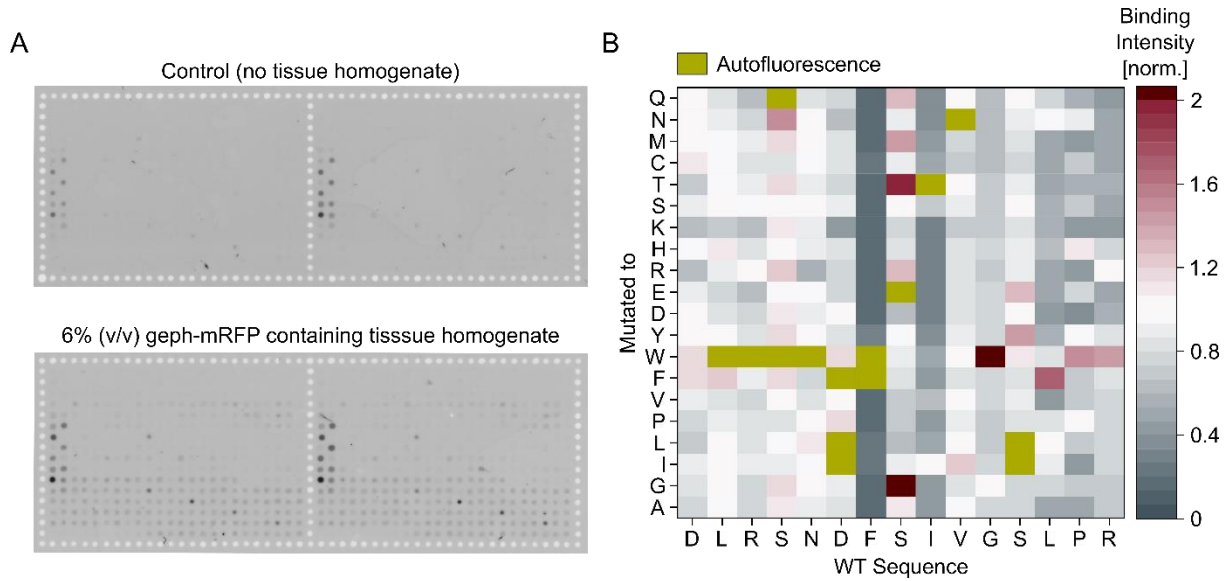
Supplemental Figure 2: Binding assays with mRFP-geph within tissue lysates from knock-in animals. Related to Figure 1 and 5. Tissue of mRFP-geph knock-in animals of 1 year of age provided by C Specht, IBENS, Paris was used directly on arrays. (A) raw readout of a microarray slide not treated with geph (upper panel) and treated with tissue lysate, containing geph fused to mRFP (lower panel). Note that autofluorescence of certain peptides in observed, while additional, geph-specific signal can be seen in the lower panel. (B) Shown are intensity values of point-mutated variants normalized to the corresponding wild-type sequence (GlyR β [414]DLRSNDFSIVGSLPR[428]) displayed as a heatmap. Higher spot intensity corresponds to preferential binding, *vice versa*. Spots that showed autofluorescence in (A) are marked in green.
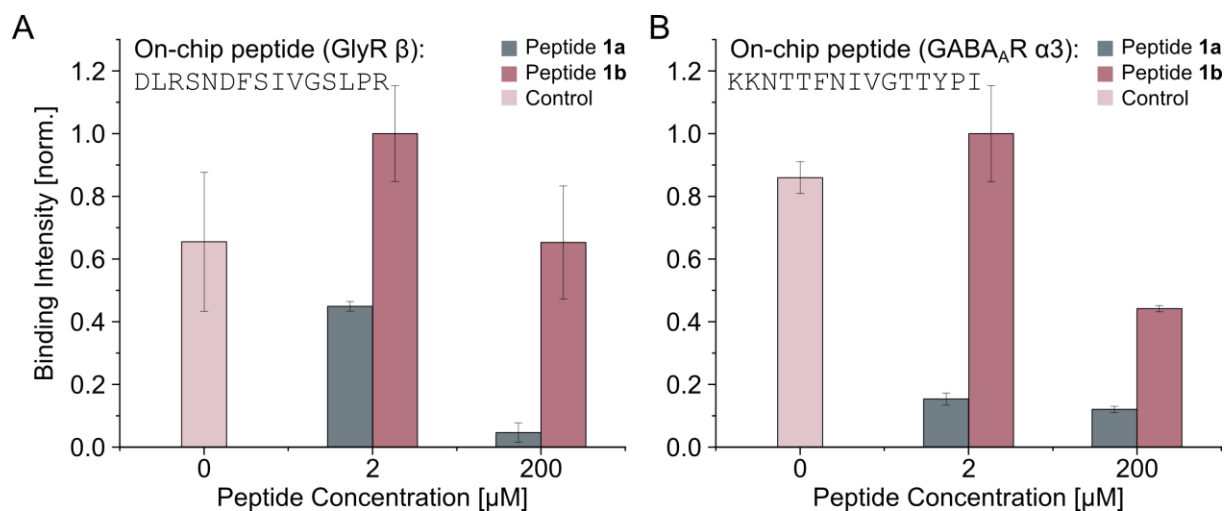
Supplemental Figure 3: In-situ on-chip peptide neutralization validates binding specificity. Related to Figure 1. gephE binding to on-chip peptides corresponding to either the GlyR β subunit (A) and the GABA$_A$R α3 subunit (B) was neutralized using peptides in solution, corresponding to either the GlyR β subunit (FSIVGSLPRDFELC, **1a**) and the GABA$_A$R α3 subunit (FNIVGTTY, **1b**). Note that to achieve neutralization of the GlyR β subunit, 200 µM of the corresponding peptide were necessary, while the GABA$_A$R subunits derived peptide could be neutralized using only 2 µM of the same peptide. Values are presented as n=2 with array internal STDEV.
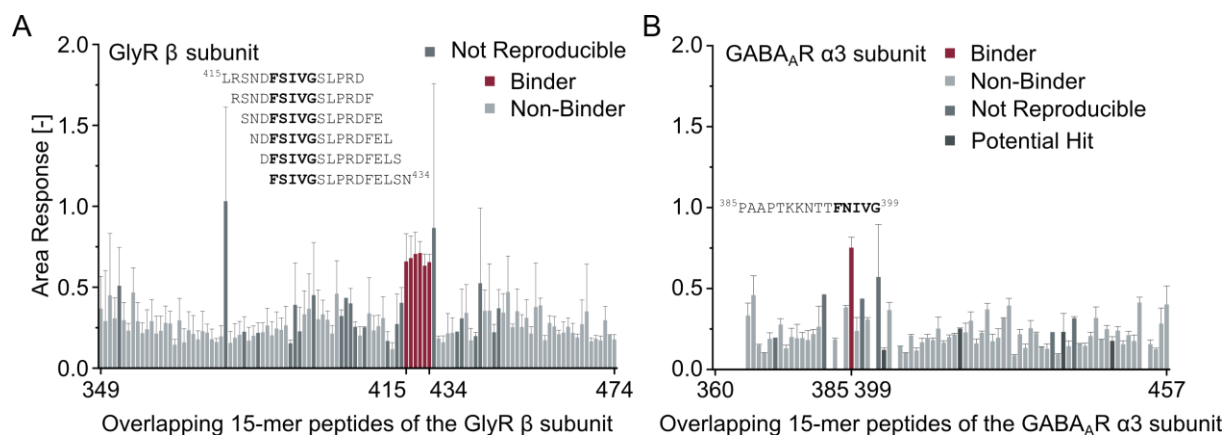
Supplemental Figure 4: Exhaustive screening of peptide libraries in solution using TRIC. Related to Figure 3. (B-C) Bar graph showing area values for each peptide measured (see Supplementary Table 3 and 4 for peptide sequences corresponding to the GlyR β (B) and GABA$_A$R α3 (C) subunit respectively and area values for each data point). Residues delimiting the peptides on-chip are represented on the x-axis. Hits are highlighted in dark red alongside corresponding peptide sequences with the respective binding motifs in bold. Note that only peptides bearing an [420]FSIVG[424] or [395]FNIVG[399] (GlyR β and GABA$_A$R α3 subunit respectively) were identified as binders. In addition to binders and non-binders, peptides classified as not reproducible or potential hits are highlighted. Values are presented as n=1-6 with corresponding STDEV if applicable.
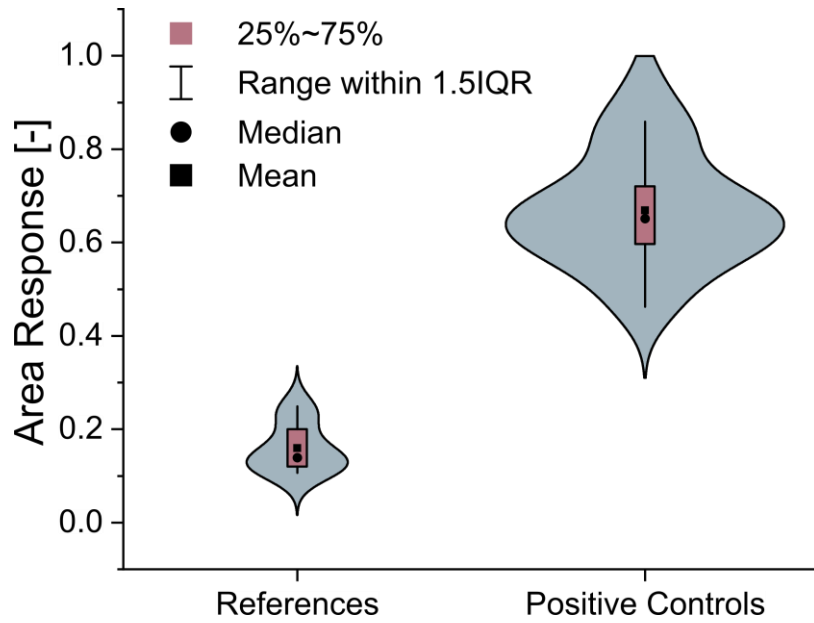
Supplemental Figure 5: Area response of reference and control measurements with unlabelled tracer. Related to Figure 3. Violin plot showing the distribution of reference measurements with no competitor peptide (n=8) and positive controls with unlabelled tracer (n=22) averaged over both 384-well plates used in single dose measurements.

240
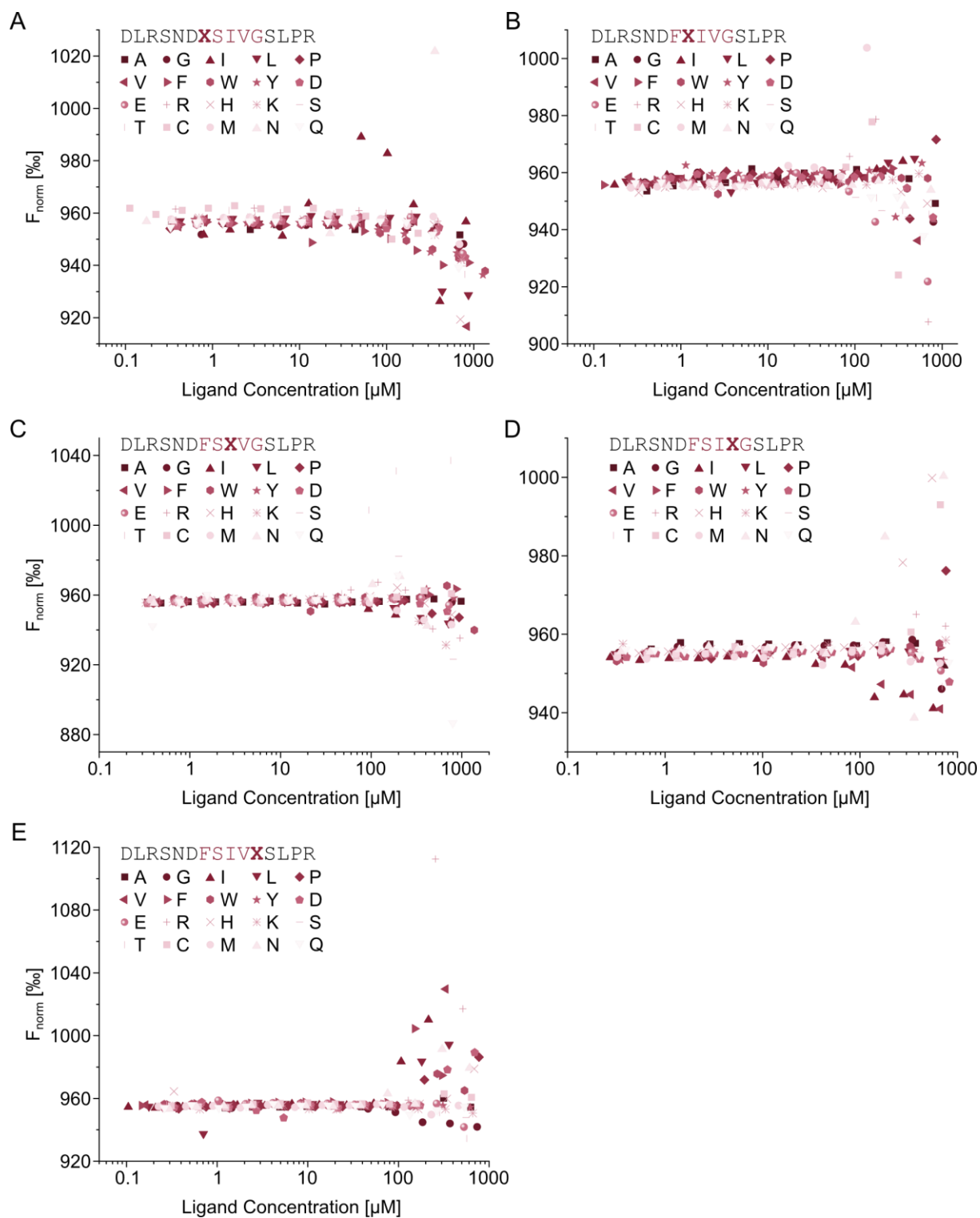
Supplemental Figure 6: Overview of all full positional scan TRIC data points. Related to Figure 5. Dose responses of 15mer peptides corresponding to variants of the core binding motif of the GlyR β subunit against geph were done in a high-throughput TRIC setup. The core binding motif is marked in red, with the variable position marked in bold. Refer to supplemental table 6 for starting concentrations and K_I values.
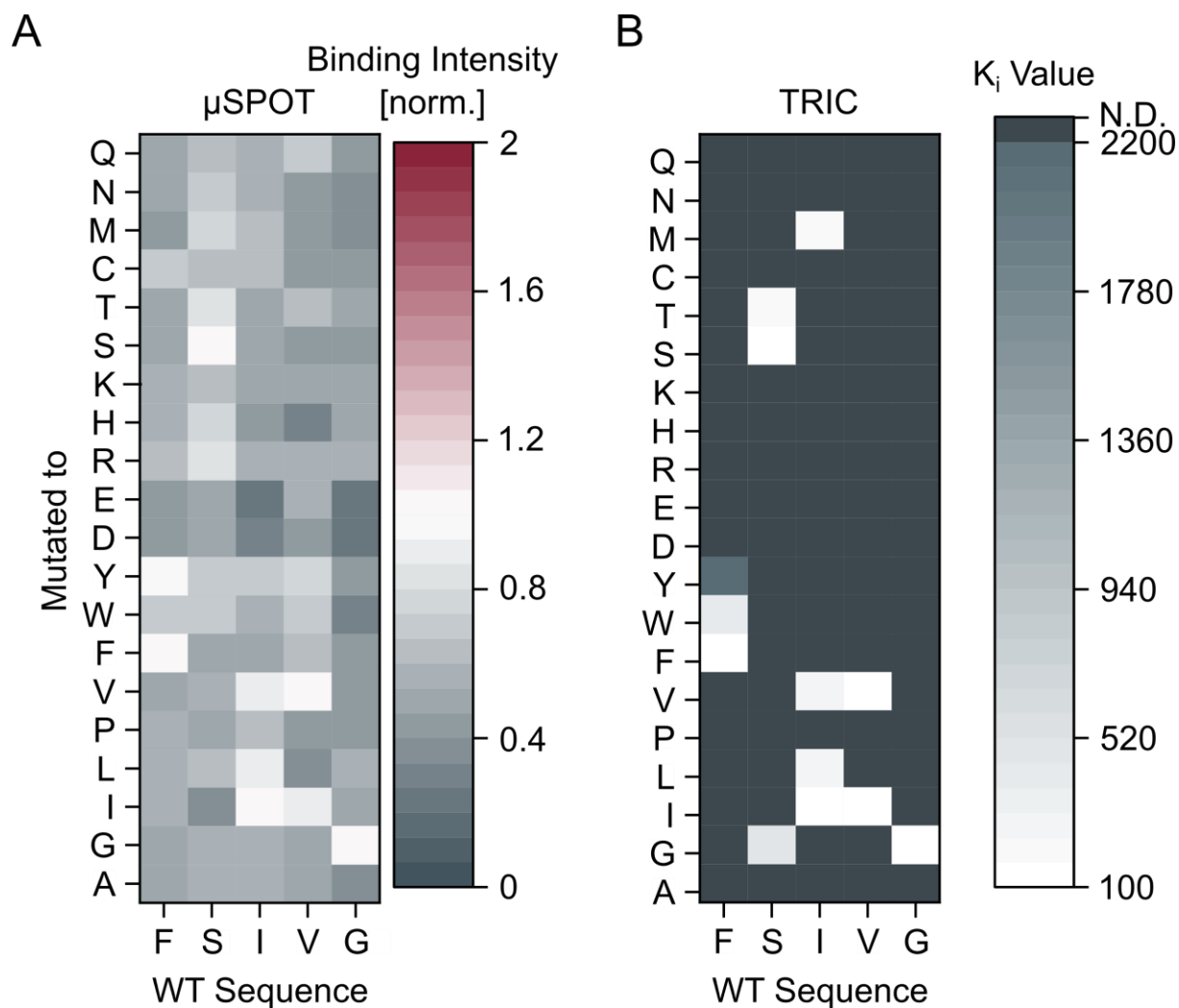
Supplemental Figure 7: Comparison of gephE/GlyR β subunit binding in μSPOT and TRIC. Related to Figure 5. (A) A full positional scanning library was probed with recombinant gephE in microarray format. Shown are intensity values of point-mutated variants normalized to the corresponding WT sequence (GlyR β [392]DLRSNDFSIVGSLPR[406]) displayed as a heatmap. Higher spot intensity corresponds to preferential binding, *vice versa*. (B) The K_i values of a peptide library corresponding to the GlyR β subunit ([414]DLRSNDFSIVGSLPR[428]), varied to every proteogenic amino acid within the FSIVG core binding motif, were determined in a TRIC displacement approach. Note that for peptides exhibiting a close to WT binding intensity in μSPOT format a K_i value could be determined in TRIC format.

Supplemental Tables

Supplemental Table 1: Overlapping peptide library corresponding to GlyR β in μSpot. Related to Figure 1. Peptide sequences are given with their delimiting residue numbers alongside the relative binding intensity and STDEV obtained for 50 nM of gephE and 3% of mouse brain lysate containing native geph.

Peptide Name/Index	Peptide Sequence	Residues	gephE Binding Intensity [norm.]	STDEV	Native geph Binding Intensity [norm.]	STDEV
Glycine receptor subunit beta_001	VVQVMLNNPKRVEAEKARIA	349-368	0.017	0.003	0.081	0.006
Glycine receptor subunit beta_002	VMLNNPKRVEAEKARIAKAE	352-371	0.010	0.003	0.082	0.001
Glycine receptor subunit beta_003	NNPKRVEAEKARIAKAEQAD	355-374	0.023	0.003	0.109	0.005
Glycine receptor subunit beta_004	KRVEAEKARIAKAEQADGKG	358-377	0.052	0.007	0.117	0.003
Glycine receptor subunit beta_005	EAEKARIAKAEQADGKGGNA	361-380	0.024	0.004	0.113	0.003
Glycine receptor subunit beta_006	KARIAKAEQADGKGGNAAKK	364-383	0.040	0.003	0.091	0.010
Glycine receptor subunit beta_007	IAKAEQADGKGGNAAKKNTV	367-386	0.025	0.005	0.066	0.010
Glycine receptor subunit beta_008	AEQADGKGGNAAKKNTVNGT	370-389	0.023	0.009	0.065	0.012
Glycine receptor subunit beta_009	ADGKGGNAAKKNTVNGTGTP	373-392	0.015	0.003	0.067	0.017
Glycine receptor subunit beta_010	KGGNAAKKNTVNGTGTPVHI	376-395	0.024	0.004	0.077	0.009
Glycine receptor subunit beta_011	NAAKKNTVNGTGTPVHISTL	379-398	0.011	0.003	0.077	0.001
Glycine receptor subunit beta_012	KKNTVNGTGTPVHISTLQVG	382-401	0.023	0.003	0.085	0.000
Glycine receptor subunit beta_013	TVNGTGTPVHISTLQVGETR	385-404	0.008	0.000	0.087	0.003
Glycine receptor subunit beta_014	GTGTPVHISTLQVGETRCKK	388-407	0.044	0.000	0.068	0.012
Glycine receptor subunit beta_015	TPVHISTLQVGETRCKKVCT	391-410	0.013	0.001	0.060	0.006
Glycine receptor subunit beta_016	HISTLQVGETRCKKVCTSKS	394-413	0.042	0.006	0.042	0.004
Glycine receptor subunit beta_017	TLQVGETRCKKVCTSKSDLR	397-416	0.016	0.003	0.054	0.020
Glycine receptor subunit beta_018	VGETRCKKVCTSKSDLRSND	400-419	0.011	0.002	0.074	0.041
Glycine receptor subunit beta_019	TRCKKVCTSKSDLRSNDFSI	403-422	0.033	0.004	0.089	0.049
Glycine receptor subunit beta_020	KKVCTSKSDLRSNDFSIVGS	406-425	0.393	0.003	0.309	0.096
Glycine receptor subunit beta_021	CTSKSDLRSNDFSIVGSLPR	409-428	0.645	0.093	0.379	0.019
Glycine receptor subunit beta_022	KSDLRSNDFSIVGSLPRDFE	412-431	0.972	0.211	0.945	0.066
Glycine receptor subunit Beta_023	LRSNDFSIVGSLPRDFELSN	415-434	1.000	0.265	1.000	0.085
Glycine receptor subunit beta_024	NDFSIVGSLPRDFELSNYDC	418-437	0.599	0.173	0.561	0.140
Glycine receptor subunit beta_025	SIVGSLPRDFELSNYDCYGK	421-440	0.291	0.143	0.301	0.019
Glycine receptor subunit beta_026	GSLPRDFELSNYDCYGKPIE	424-443	0.132	0.032	0.134	0.012
Glycine receptor subunit beta_027	PRDFELSNYDCYGKPIEVNN	427-446	0.428	0.016	0.521	0.039
Glycine receptor subunit beta_028	FELSNYDCYGKPIEVNNGLG	430-449	0.112	0.053	0.180	0.003
Glycine receptor subunit beta_029	SNYDCYGKPIEVNNGLGKPQ	433-452	0.216	0.003	0.204	0.004
Glycine receptor subunit beta_030	DCYGKPIEVNNGLGKPQAKN	436-455	0.049	0.017	0.093	0.006
Glycine receptor subunit beta_031	GKPIEVNNGLGKPQAKNKKP	439-458	0.036	0.005	0.069	0.018
Glycine receptor subunit beta_032	IEVNNGLGKPQAKNKKPPPA	442-461	0.009	0.001	0.075	0.004
Glycine receptor subunit beta_033	NNGLGKPQAKNKKPPPAKPV	445-464	0.055	0.002	0.041	0.009
Glycine receptor subunit beta_034	LGKPQAKNKKPPPAKPVIPT	448-467	0.022	0.001	0.061	0.009
Glycine receptor subunit beta_035	PQAKNKKPPPAKPVIPTAAK	451-470	0.012	0.002	0.087	0.002
Glycine receptor subunit beta_036	KNKKPPPAKPVIPTAAKRID	454-473	0.016	0.002	0.068	0.002
Glycine receptor subunit beta_037	KPPPAKPVIPTAAKRIDL	457-474	0.037	0.009	0.075	0.016

Supplemental Table 2: Overview of overlapping GABA$_A$R α3 peptide library in μSpot. Related to Figure 1. Peptide sequences are given with their delimiting residue numbers alongside the relative binding intensity and STDEV obtained for 20 nM of gephE and 6% of mouse brain lysate containing native gephyrin.

Peptide Name/Index	Peptide Sequence	Residues	gephE Binding Intensity [norm.]	STDEV	Native geph Binding Intensity [norm.]	STDEV
Gamma-aminobutyric acid receptor subunit alpha-3_001	NYFTKRSWAWEGKKVPEALE	360-379	0.062	0.005	0.048	0.022
Gamma-aminobutyric acid receptor subunit alpha-3_002	TKRSWAWEGKKVPEALEMKK	363-382	0.049	0.003	0.033	0.003
Gamma-aminobutyric acid receptor subunit alpha-3_003	SWAWEGKKVPEALEMKKKTP	366-385	0.064	0.034	0.118	0.009
Gamma-aminobutyric acid receptor subunit alpha-3_004	WEGKKVPEALEMKKKTPAAP	369-388	0.048	0.008	0.105	0.019
Gamma-aminobutyric acid receptor subunit alpha-3_005	KKVPEALEMKKKTPAAPTKK	372-391	0.038	0.007	0.081	0.023
Gamma-aminobutyric acid receptor subunit alpha-3_006	PEALEMKKKTPAAPTKKNTT	375-394	0.038	0.005	0.071	0.018
Gamma-aminobutyric acid receptor subunit alpha-3_007	LEMKKKTPAAPTKKNTTFNI	378-397	0.059	0.005	0.085	0.010
Gamma-aminobutyric acid receptor subunit alpha-3_008	KKKTPAAPTKKNTTFNIVGT	381-400	0.053	0.006	0.115	0.004
Gamma-aminobutyric acid receptor subunit alpha-3_009	TPAAPTKKNTTFNIVGTTYP	384-403	0.948	0.039	1.000	0.066
Gamma-aminobutyric acid receptor subunit alpha-3_010	APTKKNTTFNIVGTTYPINL	387-406	1.000	0.028	0.767	0.009
Gamma-aminobutyric acid receptor subunit alpha-3_011	KKNTTFNIVGTTYPINLAKD	390-409	0.443	0.018	0.243	0.006
Gamma-aminobutyric acid receptor subunit alpha-3_012	TTFNIVGTTYPINLAKDTEF	393-412	0.457	0.008	0.538	0.009
Gamma-aminobutyric acid receptor subunit alpha-3_013	NIVGTTYPINLAKDTEFSTI	396-415	0.044	0.006	0.114	0.042
Gamma-aminobutyric acid receptor subunit alpha-3_014	GTTYPINLAKDTEFSTISKS	399-418	0.030	0.004	0.098	0.058
Gamma-aminobutyric acid receptor subunit alpha-3_015	YPINLAKDTEFSTISKSAAA	402-421	0.039	0.005	0.114	0.045
Gamma-aminobutyric acid receptor subunit alpha-3_016	NLAKDTEFSTISKSAAAPSA	405-424	0.029	0.010	0.122	0.026
Gamma-aminobutyric acid receptor subunit alpha-3_017	KDTEFSTISKSAAAPSASST	408-427	0.020	0.005	0.136	0.010
Gamma-aminobutyric acid receptor subunit alpha-3_018	EFSTISKSAAAPSASSTPTA	411-430	0.028	0.003	0.127	0.000
Gamma-aminobutyric acid receptor subunit alpha-3_019	TISKSAAAPSASSTPTAIAS	414-433	0.024	0.001	0.116	0.004
Gamma-aminobutyric acid receptor subunit alpha-3_020	KSAAAPSASSTPTAIASPKA	417-436	0.030	0.001	0.103	0.031
Gamma-aminobutyric acid receptor subunit alpha-3_021	AAPSASSTPTAIASPKATYV	420-439	0.038	0.004	0.080	0.060
Gamma-aminobutyric acid receptor subunit alpha-3_022	SASSTPTAIASPKATYVQDS	423-442	0.022	0.001	0.075	0.063
Gamma-aminobutyric acid receptor subunit alpha-3_023	STPTAIASPKATYVQDSPAE	426-445	0.019	0.001	0.067	0.054
Gamma-aminobutyric acid receptor subunit alpha-3_024	TAIASPKATYVQDSPAETKT	429-448	0.018	0.004	0.060	0.032
Gamma-aminobutyric acid receptor subunit alpha-3_025	ASPKATYVQDSPAETKTYNS	432-451	0.020	0.006	0.050	0.016
Gamma-aminobutyric acid receptor subunit alpha-3_026	KATYVQDSPAETKTYNSVSK	435-454	0.070	0.001	0.059	0.022
Gamma-aminobutyric acid receptor subunit alpha-3_027	YVQDSPAETKTYNSVSKVDK	438-457	0.073	0.040	0.058	0.019

270

Supplemental Table 7: Purity of µSPOT peptides synthesized with C-terminal Rink amide linker. Related to Figure 1, 2, 3, 4 and 5. Concomitant cleavage and deprotection afforded soluble peptides which were analysed by LCMS. Protecting group by-products were not separated prior to analysis, and major impurities were identified by LCMS to be truncated sequences.

Peptide Sequence	M.W. [Da]	n	Purity [%]
Ac-SDLRSNDFSIVGSLP-NH$_2$	1604.82	2	19±1
Ac-DLRSNDFSIVGSLPR-NH$_2$	1673.88	2	39±2
Ac-LRSNDFSIVGSLPRD-NH$_2$	1673.88	2	58±2
Ac-RSNDFSIVGSLPRDF-NH$_2$	1707.87	2	45±2
Ac-KTPAAPTKKNTTFNI-NH$_2$	1629.92	2	71±13.5
Ac-TPAAPTKKNTTFNIV-NH$_2$	1600.89	2	86±1.5
Ac-PAAPTKKNTTFNIVG-NH$_2$	1556.87	2	88±3
Ac-AAPTKKNTTFNIVGT-NH$_2$	1560.86	2	84±5.5
Ac-SIVGSLPRDFELSNYDCYGK-NH$_2$	2261.08	2	51±2
Ac-GSLPRDFELSNYDCYGKPIE-NH$_2$	2301.07	2	44±8
Ac-PRDFELSNYDCYGKPIEVNN-NH$_2$	2372.07	1	73
Ac-FELSNYDCYGKPIEVNNGLG-NH$_2$	2230.04	2	47±0.5
Ac-KKKTPAAPTKKNTTFNIVGT-NH$_2$	2143.25	2	52±3.5
Ac-TPAAPTKKNTTFNIVGTTYP-NH$_2$	2120.13	2	37±3.5
Ac-APTKKNTTFNIVGTTYPINL-NH$_2$	2191.2	2	35±3.5
Ac-KKNTTFNIVGTTYPINLAKD-NH$_2$	2237.21	1	36

Supplemental References

DIKMANS, A., BEUTLING, U., SCHMEISSER, E., THIELE, S. & FRANK, R. 2006. SC2: a novel process for manufacturing multipurpose high-density chemical microarrays. *Qsar & Combinatorial Science,* 25**,** 1069-1080.

MARIC, H. M., KASARAGOD, V. B., HAUSRAT, T. J., KNEUSSEL, M., TRETTER, V., STRØMGAARD, K. & SCHINDELIN, H. 2014. Molecular basis of the alternative recruitment of GABA A versus glycine receptors through gephyrin. *Nature communications,* 5**,** 1-11.